Appl Phys B (2011) 104:161–173
DOI 10.1007/s00340-011-4514-3

Applied Physics B
Lasers and Optics

A nonlinear controller for three-dimensional tracking of a fluorescent particle in a confocal microscope

S.B. Andersson

Received: 5 September 2010 / Revised version: 19 January 2011 / Published online: 10 May 2011

Abstract We describe an algorithm for using a confocal microscope for tracking single fluorescent particles diffusing in three dimensions. The algorithm uses a standard confocal setup and directly translates each fluorescence measurement into an actuator command. Through physical simulations, we illustrate 3-D tracking in both stage scanning and beam scanning confocal systems. The simulated stage scanning system achieved tracking of particles diffusing in 3-D with coefficients up to 0.2 $\mu m^2/s$ when the average fluorescence intensities was less than 1.84 counts per measurement cycle (corresponding to less than 18,400 counts per second) in the presence of background fluorescence with a rate of 5,000 counts per second. Increasing the fluorescence intensity to approximately 193 counts per measurement cycle (1,930,000 counts per second) allowed the system to track up to particles diffusing with coefficients as large as 0.7 $\mu m^2/s$. The beam steering system allowed for faster motion of the focal volume of the microscope and successfully tracked particles diffusing with coefficients up to 0.7 $\mu m^2/s$ with fluorescence measurement intensities of approximately 0.189 counts per measurement cycle (37,570 counts per second) and with coefficients up to 90 $\mu m^2/s$ when the fluorescence intensity was increased to 19 counts per measurement cycle (3,807,500 counts/sec).

1 Introduction

The methods of single molecule spectroscopy and imaging are a class of powerful techniques in molecular biology that allow the interrogation of individual labeled proteins, viruses, and other dynamic actors important in living processes at the molecular scale. There are a variety of methods yielding subdiffraction limit position accuracy in two and three dimensions that have been described theoretically and demonstrated experimentally [1, 2]. The wide-ranging utility of such schemes can be seen in several recent review articles, including [3–6].

While approaches based on wide-field imaging have been used to great effect, they offer limited signal-to-noise ratio (SNR) and are hampered by the lack of true three-dimensional (3-D) information. As a result, several alternative methods for real-time 3-D single particle tracking have been developed. These methods generally rely on point detectors in single or multiphoton microscopes as such systems typically provide better SNR than wide-field approaches as well as 3-D sectioning capability. Information about the position of the fluorescent particle is obtained by rapidly steering the laser focus around a circle (e.g., [7, 8]), by using a scanning stage to acquire fluorescence measurements at different positions [9, 10], or by using multiple detectors to sample the fluorescence signal at different spatial positions (e.g., [11–13]). Recent reviews of the state-of-the-art of this field can be found in [5, 14, 15]. Most systems are typically able to track particles diffusing with constants of 0.1–1 $\mu m^2/s$ at high count rates, though the system reported in [8] successfully tracked quantum dots diffusing at 20 $\mu m^2/s$ (with count rates above 100,000 counts per second) while [16] tracked particles with a signal-to-background ratio as low as 2 (though with a diffusion constant of 0.5 $\mu m^2/s$ and count rates on the order of 40,000 counts per second).

These tracking schemes separate position estimation from feedback control either in space, through the use of additional hardware to sample the fluorescence intensity at

S.B. Andersson (✉)
Department of Mechanical Engineering, Boston University,
Boston, MA 02215, USA
e-mail: sanderss@bu.edu

different positions (as in [11]), in time, through the use of multiple measurements inside each controller cycle (as in [9]), or a combination of the two schemes (as in [8]). In general, the use of additional hardware increases the complexity of the system, thereby increasing the difficulty of setup and operation. Approaches that servo on the estimated position of the fluorescent particle slow down the tracking process due to the need to collect enough data for accurate estimation.

Motivated by these concerns, we introduced in [17] an alternative scheme for planar tracking which uses a standard confocal setup, requiring no additional hardware beyond a dedicated controller. The method is computationally simple and directly converts the intensity measurements into actuator commands. This is achieved through use of a reactive control law originally developed for mapping environmental quantities such as temperature, substance concentration, and radioactivity [18, 19]. The algorithm takes advantage of the geometric features of the scalar field defined by the quantity to be mapped. Its scale-invariant nature makes it well-suited for application to systems with nanometer-scale features as evidenced by its application to tracking of single particles in magnetic force microscopy [20].

In this paper, we extend the method to full 3-D tracking and, through simulation, illustrate its use. These results indicate that the scheme has the promise to achieve high-speed tracking even at low count rates, and thus at low SNR. The point spread function (PSF) and its interpretation as a scalar potential field is discussed in the next section while the tracking controller itself is introduced in Sect. 3. The simulation setup is described in Sect. 4. Because the tracking capabilities of the controller are limited primarily by the closed-loop bandwidth of the actuators, we consider both a slower scanning stage system in which motion is typically achieved using piezoelectric actuators and a faster beam steering system in which motion in the focal plane is achieved using acousto-optic modulators (AOMs) and motion along the optical axis is performed using a piezo. In each case, realistic dynamic models of the actuators are used and feedback controllers are designed to provide a large closed-loop bandwidth. The results of simulations of tracking a particle freely diffusing in 3-D are given in Sect. 5.

2 Fluorescence intensity as a spatial potential field

In a confocal microscope, fluorescence is generated by focusing an excitation source to a diffraction-limited spot in the sample. A pinhole in the conjugate focal plane spatially filters the output light, blocking the signal arising from outside the focal volume of the microscope. A detector such as an avalanche photodiode is used to measure the output fluorescence. For a single particle with a size below the diffraction limit and located at the center of the focal volume, the spatial pattern of the fluorescence is described by the point spread function (PSF),

$$I(\mu,\nu) = \big(h_{\mathrm{det}}(\mu,\nu)h^*_{\mathrm{det}}(\mu,\nu)\big)\big(h_{\mathrm{ill}}(\mu,\nu)h^*_{\mathrm{ill}}(\mu,\nu)\big), \quad (1)$$

where ill (det) denotes the illumination (detection) light [21]. Here, the amplitude point spread function is given by

$$h(\mu,\nu) = -i\frac{2\pi n A \sin^2\alpha}{\lambda} e^{\frac{i\mu}{\sin^2\alpha}} \int_0^1 J_0(\nu\rho) e^{-\frac{i\mu\rho^2}{2}} \rho\, d\rho, \quad (2)$$

where n is the refractive index of the medium in which the fluorophore is embedded, $n\sin\alpha$ is the numerical aperture (N.A.) of the objective lens, A is a scaling factor, λ is the illumination or emission wavelength, J_0 is the zeroth-order Bessel function of the first kind, and (μ,ν) are the normalized optical coordinates given by

$$\mu = \left(\frac{8\pi}{\lambda} n \sin^2\frac{\alpha}{2}\right) z, \quad (3a)$$

$$\nu = \left(\frac{2\pi}{\lambda} n \sin\alpha\right)\sqrt{x^2+y^2}. \quad (3b)$$

If the fluorescent source is at $(\Delta\mu,\Delta\nu)$ relative to the center of the focal volume, the spatial intensity is given by shifting the appropriate amplitude point spread function,

$$\begin{aligned} I(\mu,\nu;\Delta\mu,\Delta\nu) &= \big(h_{\mathrm{det}}(\mu,\nu)h^*_{\mathrm{det}}(\mu,\nu)\big)\big(h_{\mathrm{ill}}(\mu-\Delta\mu,\nu-\Delta\nu) \\ &\quad \times h^*_{\mathrm{ill}}(\mu-\Delta\mu,\nu-\Delta\nu)\big). \end{aligned} \quad (4)$$

With the pinhole in the plane defined by $\mu = 0$, the light collected by the detector, denoted I_{det}, is the integral of the intensity over the area of the pinhole combined with the background rate. That is, with r_{PH} denoting the pinhole radius,

$$I_{\mathrm{det}}(\Delta\mu,\Delta\nu) = \int_0^{r_{\mathrm{PH}}} I(0,\nu;\Delta\mu,\Delta\nu)\, d\nu + I_B, \quad (5)$$

where I_B is the background signal. Due to shot noise, the actual measured signal is a Poisson process with rate I_{det}.

The sampling process can be interpreted as measuring the value of a spatial potential field defined by the relative position of the focal point and the fluorescent particle and described by I_{det}. In the next section, we describe a controller designed to converge to a steady trajectory at a given radius from an extremum point of such a spatial potential field.

3 Tracking controller

The basic block diagram of the tracking scheme is shown in Fig. 1. For the purposes of developing a tracking controller,

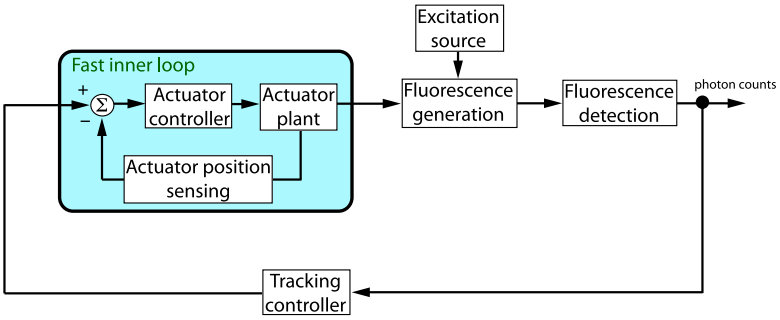

Fig. 1 Basic block diagram of the tracking scheme. The high-level tracking controller translates intensity measurements into a trajectory for the detection volume of the microscope. The low level controller should have a high bandwidth to ensure the volume accurately follows the prescribed path

we assume the existence of a low-level, high-bandwidth actuator controller and focus on trajectory determination. This low-level controller, however, should not be ignored since its speed directly limits the tracking capabilities of the overall system. Even in a beam steering system, motion along the optical axis is achieved using a piezoelectric actuator by moving either the objective lens or the sample. Because the speed of tracking is directly related to the actuation bandwidth, it is important to control the actuators with the largest possible bandwidth. While piezoelectric devices can be challenging to control due to high-order dynamics and nonlinearities such as hysteresis, there is a growing body of literature on efficient and effective controllers for these systems (see, e.g., [22–24] and discussions in [25], as well as the controller design discussed in Sect. 4.2 below).

For high-level control, we assume the motion of the center of the focal volume with respect to the sample can be modeled as

$$\dot{x} = u = (u_x \quad u_y \quad u_z)^T. \tag{6}$$

That is we assume that the low level controller will faithfully follow the trajectory commanded by the tracking controller.

Consider first tracking in the plane. To take advantage of the methods developed in [18, 19], we choose the controller form to artificially implement a nonholonomic system,

$$\begin{pmatrix} u_x \\ u_y \end{pmatrix} = v \begin{pmatrix} \cos\theta \\ \sin\theta \end{pmatrix}, \tag{7a}$$

$$\dot{\theta} = v\omega. \tag{7b}$$

Here, the steering rate, ω, is viewed as the control input. This form forces the controller to move the detection volume at a constant speed v, thereby forcing it to explore the potential field defined by I_{det}. It is shown in [19] that the control law given by

$$\omega = \frac{1}{r_o}\left(1 - K\frac{d}{dt}I_{\text{det}}\right), \tag{8}$$

with the gain K sufficiently large, converges to a distance r_o of an extremum of the potential field. Note that the time derivative is along the trajectory of the sensor (the focal point of the system in the confocal setting) and can thus be calculated directly from the measured data.

The planar tracking law converges to a periodic orbit in a plane. The first term in (8) sets the curvature, and thus the radius, of the final steady state trajectory. The second term is in essence a proportional control in which the rate of change of the intensity along the trajectory is the error that is being driven to zero.

To achieve tracking in all three dimensions, we slowly rotate the plane of the steady state trajectory about the x-axis. That is, we define the full control law as

$$\begin{pmatrix} u_x \\ u_y \\ u_z \end{pmatrix} = \begin{pmatrix} 1 & 0 & 0 \\ 0 & \cos\phi & \sin\phi \\ 0 & -\sin\phi & \cos\phi \end{pmatrix} \begin{pmatrix} v\cos\theta \\ v\sin\theta \\ 0 \end{pmatrix}, \tag{9a}$$

$$\dot{\theta} = \frac{v}{r_o}\left(1 - K\frac{d}{dt}I_{\text{det}}\right), \tag{9b}$$

$$\dot{\phi} = \omega_z, \tag{9c}$$

where ω_z is a new parameter to be chosen. To maintain stability of the overall scheme, the rotation rate of the plane should be kept slow relative to the rate of convergence of the planar control law, thereby imposing a two-time scale assumption on the controller.

To implement this law in the digital setting, we integrate (9b) and (9c) over a time step Δt to obtain the exact discretization of the angular variables

$$\theta(t + \Delta t) = \theta(t) + \frac{v}{r_o}\big(\Delta t - K\,\Delta I(t)\big), \tag{10a}$$

$$\Delta I(t) = I_{\text{det}}(t + \Delta t) - I_{\text{det}}(t), \tag{10b}$$

$$\phi(t + \Delta t) = \phi(t) + \omega_z \Delta t, \tag{10c}$$

and then input the current values into the control law in (9a).

This control law is explicitly defined by five parameters: the update rate Δt, the speed v, the gain K, the convergence distance r_o, and the rate of rotation ω_z. Implicit to the controller is the choice of an integration time on the intensity measurement. This integration time can be set to any time

up to the update rate. In general, it should be much shorter than the expected time scale of the motion to be tracked. Such a choice ensures that each intensity measurement reflects a single position of the particle rather than a sweep of positions. Shorter integration times, however, lead to a lower signal to noise ratio due to shot noise. As a result, there is a tradeoff between the speed of the controller and the accuracy of the tracking. Increasing the controller speed will lead to more variance in the trajectory due to the increased shot noise but will also allow the system to react more quickly to the motion of the particle being tracked.

The control law does not depend on any modeling parameters and thus implementation does not require detailed knowledge about the specific optical setup, about the wavelengths of light used, or about intensity levels.

3.1 Discussion

If the time scales defined by the tracking control law in (9a) and of the motion of the particle are well separated, then the trajectory of the focal point will converge to a periodic trajectory in a slowly rotating plane, essentially sweeping out a spherical shell centered on the particle (cf. Fig. 4f). The controller then reacts to the motion of the particle, shifting to keep the pattern centered on the particle.

As the two time scales become closer, this pattern breaks down and the controller reacts more directly to the motion of the particle. At high enough diffusion rates, the particle will move away from the detection volume faster than the controller can react, leading to loss of tracking. Due to the stochastic nature of Brownian motion, the time for the particle to diffuse away is a random variable. To determine whether tracking is effective, we require on average that it keep the particle in the detection range for a time longer than the expected first passage time for the particle to diffuse out of a fixed focal volume. Approximating the focal volume as an ellipsoid, this first passage time is given by

$$E[T] = \frac{1}{2D(\frac{1}{r_x^2} + \frac{1}{r_y^2} + \frac{1}{r_z^2})}, \tag{11}$$

where D is the diffusion coefficient and (r_x, r_y, r_z) are the radii of the ellipsoid approximating the detection volume [26].

Under this tracking scheme there is no explicit estimation of the position of the particle. Such estimation can be done offline, however, using a variety of known methods. In particular, the fluoroBancroft algorithm developed by the author [27] is designed to work well with only a few measurements and is well-suited to this application.

The tracking law also assumes that the low-level controller faithfully steers the focal point along the commanded trajectory. The actuator closed-loop bandwidth, then, is one of the primary limiting factors for the speed of tracking.

4 Simulation setup

To illustrate the scheme and to explore the effects of actuator dynamics and fluorescence intensity on tracking limits, the algorithm was simulated in Matlab. In all simulations, the position of the fluorescent particle, denoted x_m, was updated at a time step of δt according to a discrete time random walk given by

$$x_m(k+1) = x_m(k) + \sqrt{2D\delta t}\, w(k), \tag{12}$$

where D was the modeled diffusion coefficient and $w(\cdot)$ was a Gaussian white noise process with zero mean and unit variance. The initial position was chosen from a uniform distribution in a cube with 100 nm edges centered at the origin. The value of δt was selected in each simulation run to be faster than the update rate of the controller.

4.1 Generation of fluorescence measurements

The optical parameters of the system were set to a N.A. of 0.8, a pinhole size of 20 μm, an excitation wavelength of $\lambda_{\text{ill}} = 408$ nm, and an emission wavelength of $\lambda_{\text{det}} = 505$ nm. The surrounding media was assumed to be water and so the index of refraction was set to $n = 1.333$. The background rate was set to 0.2 of the peak intensity level selected for the run. These parameters (except for the background rate) were used in (5) to generate the noise free-intensity at a given relative displacement of the center of the focal spot and the position of the particle. The radius to the first minimum of the PSF in the plane (denoted r_x and r_y) and along the optical axis (denoted r_z) were given by [28]

$$r_x = r_y = \frac{0.61\lambda_{\text{det}}}{\text{N.A.}} = 0.3851\ \mu\text{m}, \tag{13a}$$

$$r_z = \frac{2\lambda_{\text{det}} n}{\text{N.A.}^2} = 2.105\ \mu\text{m}. \tag{13b}$$

As seen in (5), the intensity depends only on the relative separation in the plane and along the optical axis. To speed up the simulation, noise-free intensity values were precomputed along a grid spanning 0 to $1.5r_x$ in the longitudinal direction and 0 to $1.5r_z$ in the axial direction, with 5 nm resolution in the planar axis and 10 nm resolution along the optical axis. Intermediate values were calculated using interpolation based on Delaunay triangulation. At run time, the distance between the focal point and the particle was calculated and the noise free sample was determined by scaling the interpolated values. To model shot and background noise, the simulated intensity was generated by sampling from a Poisson distribution with a rate given by the sum of the noise-free intensity and the background rate. Simulated images of the noise free and noisy PSF are shown in Fig. 2.

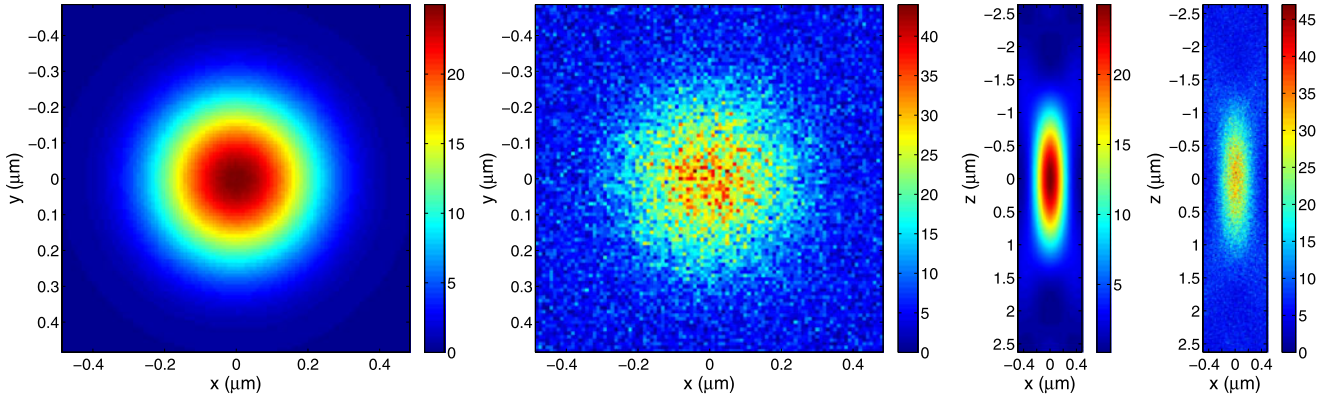

a PSF in the focal plane **b** PSF along the optical axis

Fig. 2 Simulated PSF images generated from (5) using the parameters: N.A. = 0.8, pinhole = 20 μm, $n = 1.333$, $\lambda_{\text{ill}} = 488$ nm, and $\lambda_{\text{det}} = 505$ nm. The noise-free intensity in these images was scaled to produce a peak of 20 counts and the background rate was set to 4 counts. The PSF is shown in the (**a**) focal plane and (**b**) in a plane along the optical axis. In each case the *left* image is the noise-free PSF and the *right* image is the noisy PSF generated by sampling from a Poisson distribution with a rate given by the noise-free values plus the background rate

4.2 Actuators

Simulation were performed with two different styles of actuation, a scanning stage system in which a three-axis nanopositioning stage was used to move the sample relative to the focal point of the microscope and a beam scanning system in which relative motion in the focal plane was achieved by steering the excitation beam using AOMs and motion along the optical axis was achieved by using a piezoelectric actuator to move the sample.

4.2.1 Stage-scanning system

The stage scanning system was modeled after a Mad City Labs Nano-PDQ nanopositioning stage. The stage dynamics in open loop of the physical scanner were identified in each axis using a swept-sine approach (due to the frame-in-frame design of the stage, the three directions operate nearly independently). The system identification toolbox in Matlab was used to fit transfer function models to the data.

Closed-loop controllers for each axis were designed based on the identified models. In each case, the two main resonances were cancelled using a tuned proportional-integral-derivative (PID) controller (described in [24]), a lead controller was added for stability (see, e.g., [29]), and a high-order low pass filter was included for adequate high-frequency roll-off. In the case of the y-axis, an additional term was added to cancel the highest-frequency zero and pole. The controllers achieved closed-loop bandwidths of 1.68 kHz in the x-, 1.57 kHz in the y- and 501 Hz in the z-directions. The Bode plots of the plant, controller, and closed-loop systems for the three axes are shown in Fig. 3.

4.2.2 Beam-scanning system

The beam scanning system was modeled on the use of a pair of AOMs to steer the beam in the focal plane and a single axis piezoactuator to move the sample along the optical axis. The bandwidth of an AOM is typically in the MHz range and so for the purposes of these simulations we assigned them a unity transfer function. Commercially available z-axis piezoactuators have high resonant frequencies. Examples include the NanoHSZ from Mad City Labs (Madison, WI, USA) with an unloaded resonant frequency of 7.5 kHz and the NPZ25A from nPoint (Middleton, WI, USA) with an unloaded resonant frequency of 4 kHz. To capture the dynamics of such actuators, we utilized a standard second-order transfer function model

$$G_{z_{\text{fast}}}(s) = \frac{\omega_n^2}{s^2 + 2\zeta\omega_n s + \omega_n^2} \tag{14}$$

with a resonant frequency of $\omega_n = 5.00$ kHz and a damping ratio of $\zeta = 0.01$. The closed-loop controller was designed using a tuned PID controller [24], yielding a closed-loop bandwidth of 25 kHz.

5 Simulation experiments

5.1 Sample run with a fixed particle

To illustrate the motion of the focal point generated by the tracking control law, a 200 millisecond tracking run based on the stage-actuated system was simulated. The particle was held fixed at an initial position chosen randomly from

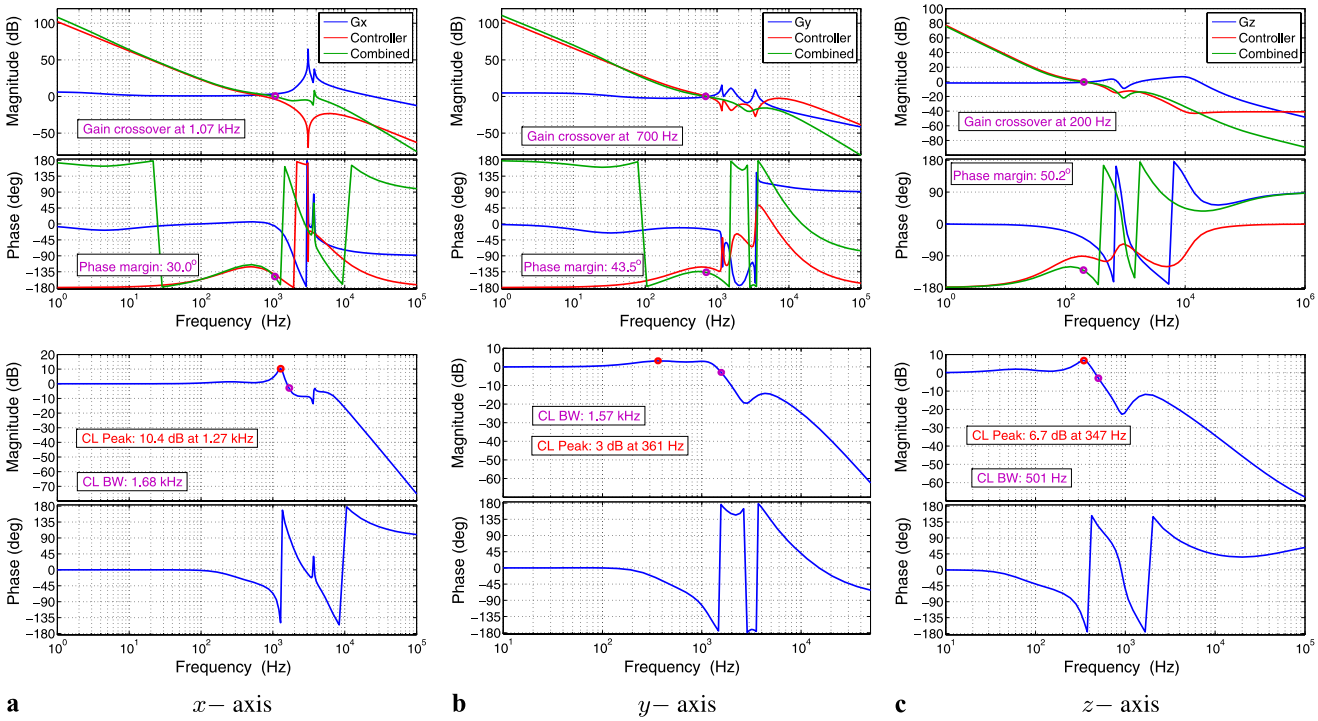

Fig. 3 Bode plots of nanopositioning stage and controllers in the (**a**) x-, (**b**) y-, and (**c**) z-directions used in the stage-scanning system simulations. In each case the top plot shows the actuator model (*blue*), the designed controller (*red*), and the combined (open loop) model, and includes the crossover frequency and phase margin of the controller and actuator. The *bottom plot* shows the closed loop response and includes the closed loop bandwidth and peak gain. The actuator models were identified from a Mad City Labs Nano-PDQ 3-axis nanopositioning stage

a uniform distribution on a cube centered at the initial location of the focal point and with 100 nm sides. The intensity scaling was set to yield a noise-free peak intensity of 100 counts/ms and the background fluorescence rate was set to 20 counts/ms. The controller update period was set to $\Delta t = 100$ µs (for a controller sampling rate of 10 kHz). The simulator was updated every $\delta t = 5$ µs. The steady state radius was set to $r_o = 0.155$ µm. The speed of the motion of the focal point was set to $v = 115$ µm/s, corresponding to 118 revolutions/s around the steady-state circle, while the speed of rotation of the plane of convergence was set to $\omega_z = 350$ rad/s, corresponding to 111 revolutions/s. The gain was set to $K = 0.11$. (For a discussion on selecting the controller parameters, see Sect. 5.4.) The results of the simulation are shown in Fig. 4.

The 3-D trajectory of the focal point in Fig. 4(f) illustrates the steady-state motion about the fluorescent particle. The convergence of the overall pattern to the desired radius from the particle can be seen clearly in the x-trajectory in Fig. 4(a). Over the first few cycles, the entire oscillatory pattern shifted upward until the particle position was at the center. Due to the rotation of the plane of convergence, the trajectory in the y- and z-axes, shown in Figs. 4(b, c) was more complicated. As expected, the convergence of the z-trajectory to an average position centered on the particle was significantly slower than in the other two directions. Note that the plots show the actual actuator trajectories and not the commanded values. They therefore reflect the dynamics of the piezoelectric actuators captured by the transfer function models as well as the motion commanded by the tracking control law.

The rotation of the plane of convergence was also reflected in oscillations in the distance between the focal point and the particle, shown in Fig. 4(d). The mean distance over the simulation run was 0.1927 µm, somewhat larger than chosen radius of 0.155 µm. This difference was driven primarily by the shot and background noise in the intensity measurements. Note also that the rate of convergence of the radius was limited by that of the slowest axis, the z-direction.

The measured counts, shown in Fig. 4(e), ranged from zero to 20 in each measurement cycle, with an average intensity measured per controller period of 8.07 counts/100 µs, corresponding to 80,700 counts/s. The stochastic nature of the signal was driven primarily by the shot noise and background noise.

5.2 Sample runs with $D = 0.1$ µm^2/s

To illustrate the system tracking a diffusing particle, a five-second tracking run was run based on the stage-scanning

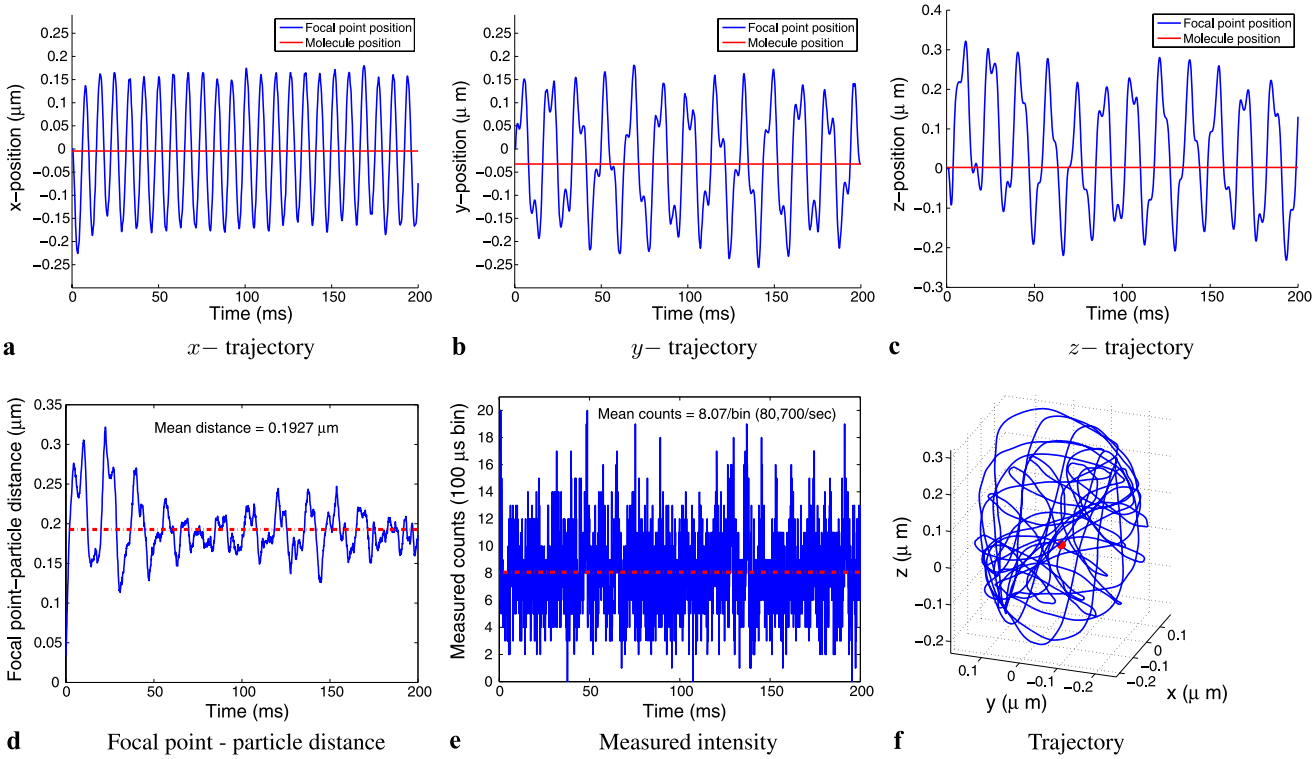

Fig. 4 Simulation run on a fixed particle using the stage scanning system. The controller parameters were set to $r_o = 0.155$ μm, $K = 0.11$, $v = 115$ μm/s, and $\omega_z = 350$ rad/s. (**a**–**c**) show the actuator (*blue*) and particle (*red*) trajectories in each of the three directions. The resulting 3-D trajectory of the focal point is shown in (**f**). The trajectories illustrate fast convergence in the (x, y)-directions and somewhat slower convergence in the z-direction and illustrate the rotation of the focal point around the fluorescent particle. The distance between the focal point and the particle is shown in (**d**). The mean distance was 0.1927 μm, somewhat larger than the designed $r_o = 0.155$ μm, driven both by the rotation of the plane of convergence and the shot and background noise in the measurements. The measured intensity, shown in (**e**), averaged 8.07 counts/100 μs sampling period, corresponding to 80,700 counts/s

system with a particle freely diffusing in 3-D with a coefficient of diffusion of $D = 0.1$ μm^2/s. The intensity and controller parameters were set as in the fixed-particle case. The results are shown in Fig. 5. The x- and y-trajectories in Figs. 5(a, b) showed good tracking performance, with the particle kept at the center of the focal point trajectory. The tracking in the z-axis, shown in Fig. 5(c), was poorer. A 400 ms portion of the particle trajectory and the trajectory of the focal point are shown in Fig. 5(f). The tracking error along the optical axis was directly reflected in the fluctuations in the focal-point particle distance, shown in Fig. 5(d). The measured fluorescence intensity, shown in Fig. 5(e), ranged from 0 to 25 counts per measurement cycle and the average fluorescence intensity per controller period during the run was 7.987 counts, corresponding to 79,865 counts/s. The untracked motion of the particle led to increased variance in the measured intensity with respect to the fixed-particle case.

There are likely two causes for the poorer tracking along the optical axis. The first is that the feedback bandwidth of the actuator in this direction was significantly slower than those of the actuators in the planar axes, 501 Hz as opposed to 1.68 kHz in x and 1.57 kHz in y. As a result, the actuator was unable to respond as quickly to the intensity variations in this direction. This can be overcome through the use of faster actuators (cf. Sect. 5.3).

The second reason is the fact that the PSF was broader along the optical axis then in the planar directions (see Fig. 2). This implies that the rate of change of the intensity along the optical axis was slower than in the lateral directions, leading to a smaller value of the derivative of the intensity along this direction. As seen from the control law in (9b), this produces a slower response along this axis. Tracking performance could likely be improved by adapting the radius of the steady-state trajectory based on the current orientation of the plane in which the trajectory lies, so as to maximize the derivative of the intensity as the focal point is moved off the steady-state trajectory.

5.3 Sample run with the beam scanning system

When tracking faster particles, the performance can be improved by increasing the control rate and using faster actuators. To illustrate this, a five second tracking run with

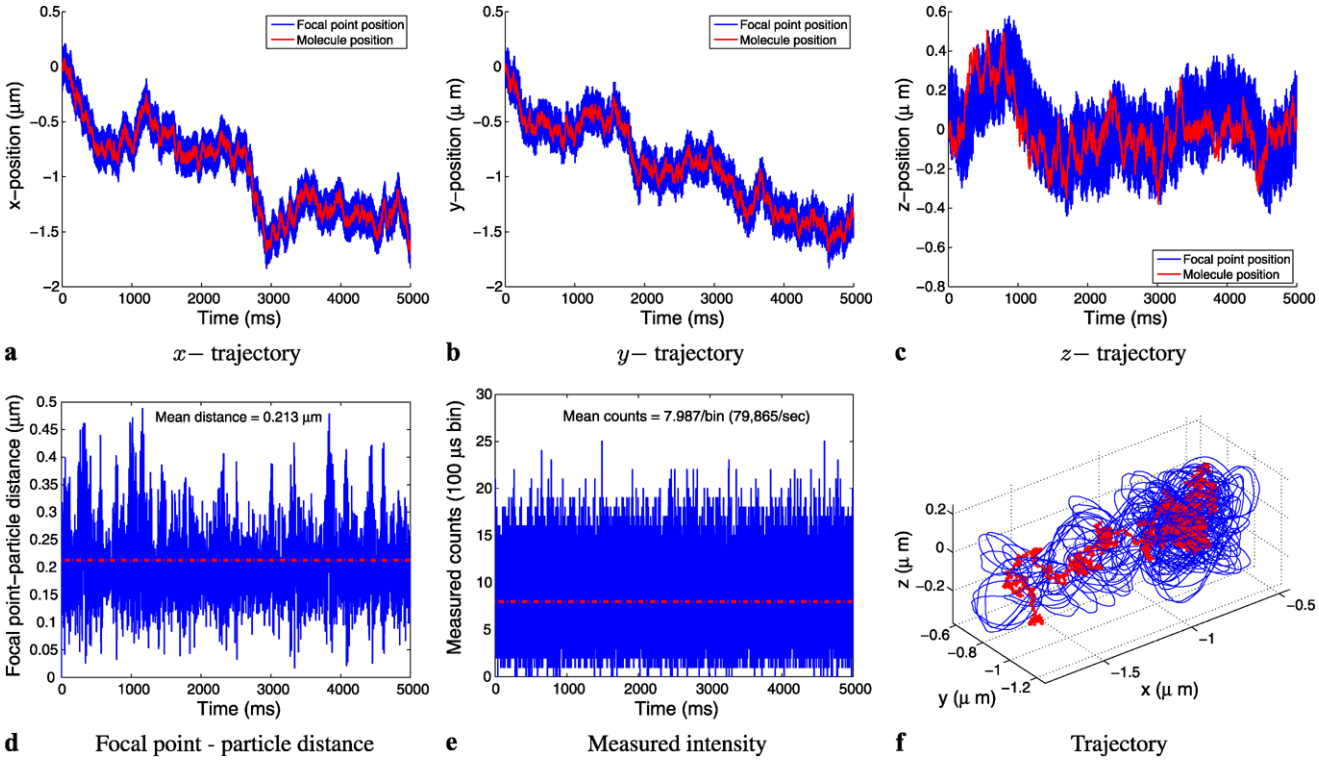

Fig. 5 Simulation run using the stage scanning system to track a particle freely diffusing in 3-D with $D = 0.1$ μm^2/s. The controller parameters were set to $r_o = 0.155$ μm, $K = 0.11$, $v = 115$ μm/s, and $\omega_z = 350$ rad/s. (**a**–**c**) show the actuator (*blue*) and particle (*red*) trajectories in each of the three directions. Tracking performance was good in the planar directions but poorer in the axial direction due to the slower dynamics in that axis and to the differences in the PSF of the optical system. This increased error was directly reflected in the distance between the particle and focal point, shown in (**d**). The mean distance over the run was 0.213 μm, significantly larger than the designed distance of 0.155 μm. The measured counts are shown in (**e**). The mean measured value in the run was 7.99 counts/100 μs sample period, corresponding to 79,865 counts/s. A 0.4 second-portion of the 3-D particle trajectory (*red*) and focal point trajectory (*blue*) is shown in (**f**). As with the fixed particle, the circular trajectory of the focal point as well as the rotation of the plane of convergence can be seen

a particle moving with the same diffusion coefficient as in the previous simulation ($D = 0.1$ μm^2/s) but using the beam scanning system was performed. The controller update period was reduced to 5 μs (corresponding to 200 kHz) and the simulator update period was reduced to 2.5 μs (corresponding to 400 kHz). Given the extremely fast dynamic response of the AOMs for beam steering, the speed of the focal point was increased to 7800 μm/s, corresponding to 7,760 revolutions/s. Similarly, the z-actuator of the beam steering system was much faster than that of the stage scanning system and thus the speed of rotation of the plane of convergence was increased to $\omega_z = 10000$ rad/s, corresponding to 3183 revolutions/s. The gain was set to $K = 0.00145$ and the steady-state radius to $r_o = 0.16$ μm. The results of the simulation are shown in Fig. 6.

The tracking in the planar directions, shown in Figs. 6(a, b), was again good, with the particle kept in the center of the focal point pattern. Tracking along the optical axis, shown in Fig. 6(c) was slightly improved relative to the stage actuated system, though still poorer than in the lateral directions. A 10 ms snapshot of the trajectory of the particle and the motion of the focal point, shown in Fig. 6(f), clearly indicates the circular motion of the focal point around the particle. (Note that the 10 ms time contains the same number of sample points as the 200 ms snapshot shown in the stage-actuated system example run in Fig. 5(f).) The improved tracking reduced the mean distance between the focal point and the particle, Fig. 6(d) to 0.201 μm as compared to the 0.213 μm in the stage scanning case. The measured intensity, shown in Fig. 6(e), had an average counts per period of 0.4339 counts/period, corresponding to 86,780 counts/s.

The ability to improve tracking performance by increasing the controller rate is limited by the fluorescence intensity. As the controller rate is increased, the sampling time is decreased, reducing the measured intensity in each sample period. This can be compensated by increasing the power of the excitation source to increase the fluorescence intensity at the cost of an increased rate of photobleaching.

It should be noted that a controller rate of 200 kHz is quite fast. While the control laws presented here are computationally simple, to achieve such rates would likely require

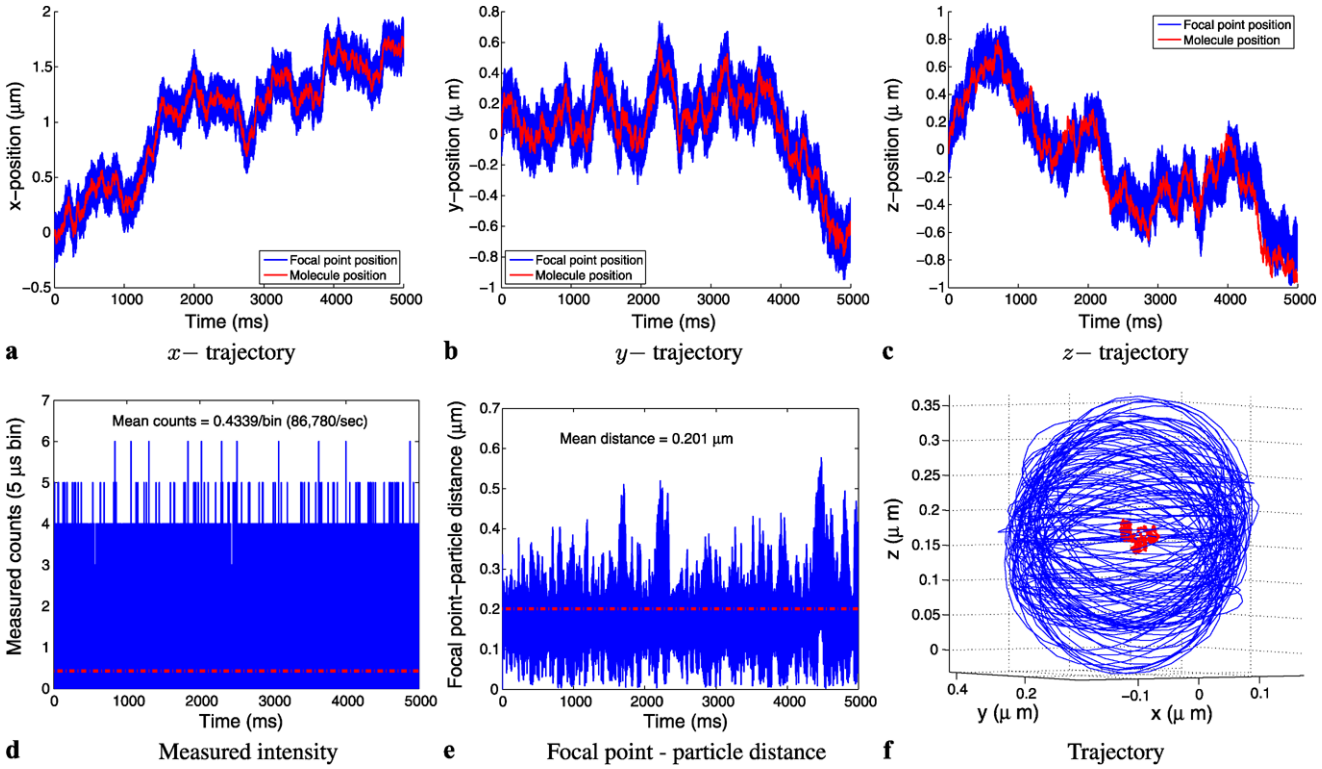

Fig. 6 Simulation run using the beam scanning system tracking a particle freely diffusing in 3-D with $D = 0.1$ μm^2/s. The controller parameters were set to $r_o = 0.16$ μm, $k = 0.00145$, $v = 7800$ μm/s, and $\omega_z = 10000$ rad/s. (**a**–**c**) show the actuator (*blue*) and particle (*red*) trajectories in each of the three directions. As before, tracking performance was poorer in the axial direction than the lateral direction due to the slower dynamics in that axis and to the differences in the PSF of the optical system. The distance between the particle and focal point is shown in (**d**). The mean distance over the run was 0.201 μm, significantly larger than the designed distance of 0.155 μm but closer than when the stage-actuated system was used (see Fig. 5). The measured counts are shown in (**e**). The mean measured value in the run was 0.4339 counts/5 μs sample period, corresponding to 86,780 counts/s. A 10 ms-portion of the 3-D particle trajectory (*red*) and focal point trajectory (*blue*) is shown in (**f**). Since the controller dynamics are now significantly faster than those of the particle, the circular trajectory, and the rotation of the converging plane are clearly evident

the use of a field programmable gate array (FPGA) system or similar high throughput system.

5.4 Parameter selection

The performance of the tracking control law is influenced by the choice of the parameters. To illustrate the effect of varying these parameters, simulations were performed in which one parameter was varied while the others were held fixed. Because it is expected that the optimal choice of values with respect to the ability to track diffusing particles depends in part on the speed of the tracking algorithm, two sets of simulations were performed, one for the stage-actuated system and one for the beam-scanning system.

For the stage-actuated system, the controller sample rate was set to 10 kHz, the diffusion coefficient of the particle to 1.0 μm^2/s, the peak noise-free intensity rate to 500 counts/ms, and the background noise rate to 100 counts/ms. Each simulation was run until tracking was lost. Five simulation runs were performed for each parameter value and the tracking time averaged over those runs. The results are shown in Fig. 7. From these simulations, the control parameters for the stage-actuated system were set to $r_o = 0.155$ μm, $K = 0.11$, $v = 115$ μm/s, and $\omega_z = 350$ rad/s. These parameters correspond in steady state to 118 revolutions/s of the focal point in the plane and 111 revolutions/s of the plane of convergence.

For the beam-actuated system, the controller sample rate was set to 200 kHz, the diffusion coefficient to 15 μm^2/s, the peak noise-free intensity rate to 5000 counts/ms, and the background noise rate 1000 counts/ms. As before, five simulation runs were performed for every parameter value. The results are shown in Fig. 8. From these simulations, the control parameters were set to $r_o = 0.16$ μm, $K = 0.00145$, $v = 7800$ μm/s, and $\omega_z = 10000$ rad/s. These parameters correspond in steady state to 7,760 revolutions/s of the focal point in the plane and 3183 revolutions/s of the plane of convergence.

While here the parameters were varied individually, the optimization of the parameter values should be done jointly as one expects their effect to be coupled. Similarly, the op-

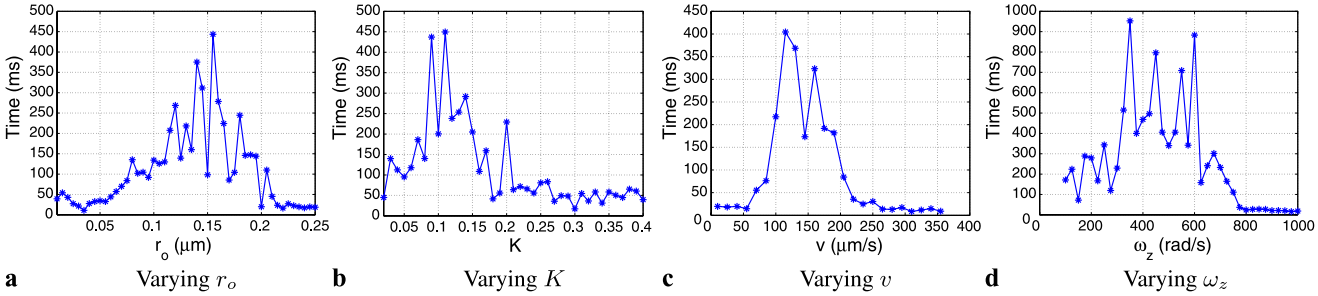

Fig. 7 Effect of control parameter selection on tracking with the stage-actuated system. The maximum tracking time (averaged over five runs) change as each parameter was varied. In each case, other control parameters were held fixed. The diffusion coefficient was set to 1.0 μm^2/s

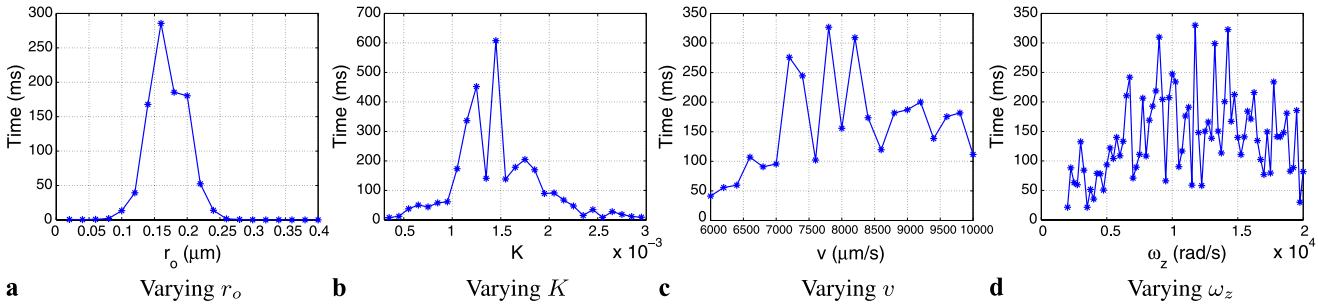

Fig. 8 Effect of control parameter selection on tracking with the beam-actuated system. The maximum tracking time (averaged over five runs) change as each parameter was varied. In each case, other control parameters were held fixed. The diffusion coefficient was set to 15 μm^2/s

timal values are likely to depend upon system parameters such as the intensity level and the diffusion coefficient. In general, a theoretical understanding of the role of the control law parameters is needed to best guide their selection.

5.5 Tracking limits

To explore the effectiveness of the proposed control law, we performed simulations for particles diffusing at a range of different diffusion coefficients using both the stage scanning and beam scanning systems and for low and high intensity levels. The values of the controller parameters were selected based on the results of Sect. 5.4. At each value of the diffusion coefficient, 10 tracking runs were performed. Each simulation was run until tracking failed, up to a maximum of five seconds of simulated time. Tracking in a run was declared failed if the particle moved out of the ellipsoid defined by the radii r_x, r_y, and r_z given in (13). In each run, the initial position of the particle was chosen randomly from a uniform distribution on a cube with 200 nm sides and centered at the initial position of the focal volume.

At each value of D, the tracking time, the measured counts, and the distance between the particle and the focal point were averaged over the 10 runs. The algorithm was considered to have successfully tracked a particle at a given value of D if the averaged tracking time was greater than the expected first passage time for the particle to diffuse out of a fixed ellipsoidal volume (defined by the radii in (13)), calculated from (11).

5.6 Stage scanning system

For the stage scanning system, the controller update rate was set to 10 kHz and the simulation rate to 200 kHz. The speed of the focal point was set to 115 μm/s (corresponding to 118 revolutions/s in steady state) and the speed of rotation of the plane of convergence was set to 350 rad/s (corresponding to 111 revolutions/s). The gain was set to $K = 0.11$ and the radius to $r_o = 0.155$ μm. For the low intensity case, the peak noise-free rate from the particle was set to 25 counts per ms and the background rate to 5 counts per ms. For the high intensity case, the peak noise-free rate from the particle was set to 2500 counts per ms and the background rate to 500 counts per ms. The results based on the stage scanning system are shown in Fig. 9.

The average tracking time as a function of diffusion coefficient is shown in Fig. 9a. Also shown on the plot is the expected first passage time for the particle to diffuse out of the (fixed) focal volume, calculated according to (11). Under both intensity levels, the system successfully tracked for the full five seconds at low values of D. At the lower intensity level, the total tracking time began to fall off at a value

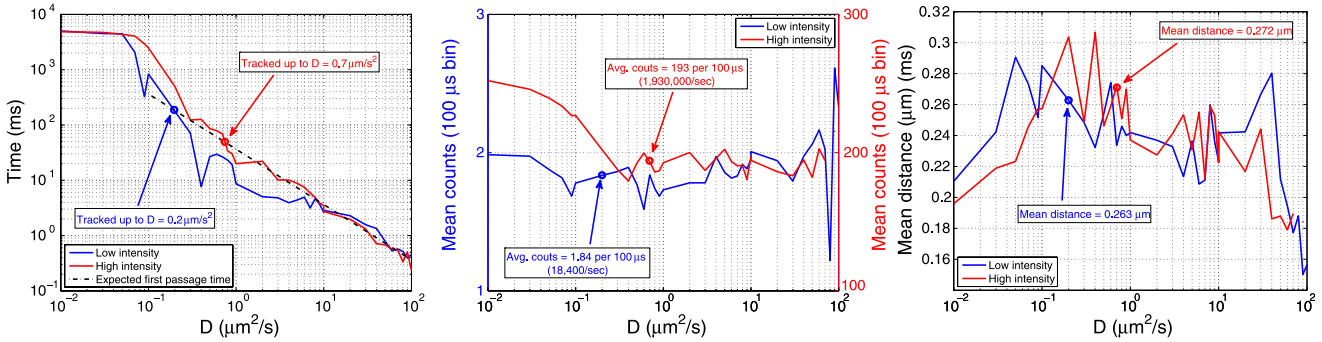

Fig. 9 Simulation results for the stage scanning system. (**a**) Tracking time as a function of diffusion coefficient for both low (*blue solid line*, *left*) and high (*red solid line*, *red*) fluorescence intensities. The expected first passage time (*black dashed line*) is also shown. (**b**) Mean intensity as a function of diffusion coefficient. *Arrows* indicate the mean intensity at the highest values of D at which successful tracking was achieved. (**c**) Mean distance between the particle and the center of the focal volume as a function of diffusion coefficient. *Arrows* indicate the mean distance at the highest values of D at which tracking was achieved. See text for discussion

of approximately $D = 0.05$ μm^2/s and remained above the expected first passage line up to $D = 0.2$ μm^2/s (with a dip at $D = 0.09$ μm^2/s). Tracking performance was slightly better with the higher intensity. The total tracking time began to fall off at a value of $D = 0.07$ μm^2/s and remained above the expected first passage line up to $D = 0.7$ μm^2/s. The shape of the two curves was quite similar, indicating that increasing the intensity directly increased the tracking time at a given value of D. The performance increase was not large, however, given the two orders-of-magnitude increase in the fluorescence level, indicating that this tracking system is being limited primarily by the dynamics of the actuators.

The average intensity across the 25 tracking runs at each value of D is shown in Fig. 9b, with the left vertical axis corresponding to the low intensity runs and the right vertical axis to the high intensity runs. The behavior of the measured intensity was similar in both cases, falling off as D was increased until tracking failed, reflecting the fact that the particle was not kept at the center of the focal volume (see also the mean distance shown in Fig. 9c). At values of D larger than the tracking limit, the mean intensity remained relatively constant or even increased with increasing D. This was due to the fact that the particle diffused away from the focal volume faster, yielding fewer measurements before the particle diffused out of the detection volume. Since on average, the particle began at the center of the detection volume, the average intensity was higher.

The average distance between the center of the focal volume and the particle during the tracking runs is shown in Fig. 9c. The mean distance initially increased with increasing D, indicating a decrease in tracking performance. At larger values of D, the mean distance began to decrease due to the fact that the particle was more likely to diffuse away from the volume within the controller update time, preventing the system from reacting to the motion and causing loss of tracking earlier. Similar to the intensity results, since the average initial particle position was at the center of the focal volume, the reduced number of measurements led to the decrease in the average distance.

In the low intensity case, successful tracking was achieved with average measured counts of less than 2 counts per 100 μs sampling period or, equivalently, less than 20,000 counts/sec. Tracking at even lower counts can be achieved by trading off fluorescence intensity for tracking time and tracking error.

5.7 Beam scanning system

The results based on the beam scanning system are shown in Fig. 10. The controller update rate was set to 200 kHz and the simulation rate to 400 kHz. The speed of the focal point was set to 7800 μm/s, corresponding to 7760 revolutions/s, and the speed of rotation of the plane of convergence was set to $\omega_z = 10000$ rad/s, corresponding to 3183 revolutions/s. The gain was set to $K = 0.00145$ and the radius to $r_o = 0.16$ μm. Two intensity levels were considered, one with a peak rate of 50 counts per ms (with a background rate of 10 counts per ms) and one with a peak rate of 5,000 counts per ms (with a background rate of 1,000 counts per ms).

The average tracking time as a function of diffusion coefficient is shown in Fig. 10a. With the lower intensity, tracking was achieved for the full five seconds up to $D = 0.2$ μm^2/s and the tracking time remained greater than the expected first passage line up to $D = 0.7$ μm^2/s. (These numbers are not a significant improvement over the stage scanning case, indicating that in the low intensity case tracking was being limited not by the actuator dynamics but by the signal level.) At the higher intensity level, tracking was achieved for the full five seconds at diffusion coefficients up to $D = 6$ μm^2/s and the tracking time remained greater than the expected first passage time up to $D = 90$ μm^2/s.

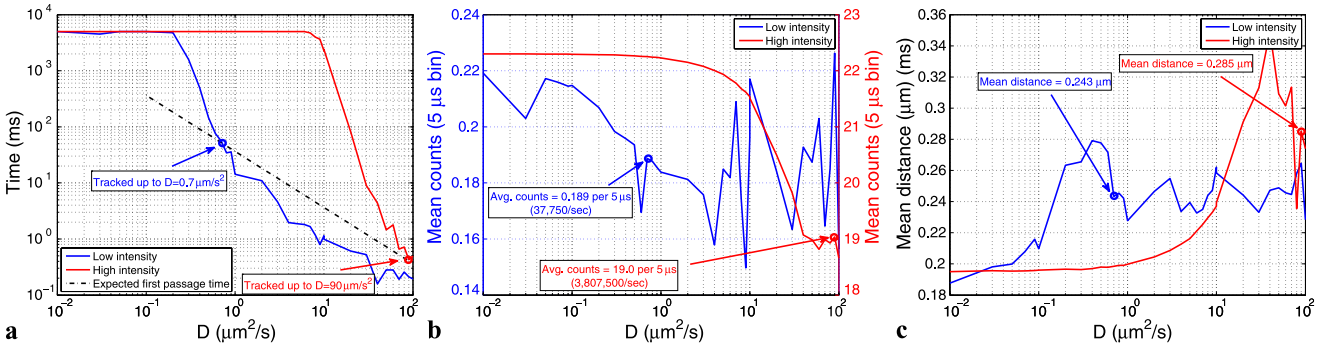

Fig. 10 Simulation results for the beam scanning system. (**a**) Tracking time as a function of diffusion coefficient for both low (*blue solid line*, *left*) and high (*red solid line*, *red*) fluorescence intensities. The expected first passage time out of the focal volume (*black dashed line*) is also shown. (**b**) Mean intensity as a function of diffusion coefficient. *Arrows* indicate the mean intensity at the highest values of D at which successful tracking was achieved. (**c**) Mean distance between the particle and the center of the focal volume as a function of diffusion coefficient. *Arrows* indicate the mean distance at the highest values of D at which tracking was achieved. See text for discussion

The average measured intensity as a function of diffusion coefficient is shown in Fig. 10b. For the low intensity case, the average measured intensity for the lowest values of D considered was 0.22 counts/5 μs sampling period, corresponding to 44,000 counts/s. At loss of tracking, this had dropped to 0.189 count/5 μs sampling period, corresponding to 37,750 counts/s. In the high intensity case, the mean intensity remained constant at 22.2 counts/5 μs (4,440,000 counts/s) up to approximately $D = 0.4$ μm^2/s, indicating good tracking across this range of diffusion coefficients. As D was increased, the mean intensity began to fall. At loss of tracking, the mean intensity was approximately 19 counts/5 μs (3,800,000 counts/s). As before, these values reflect the background noise as well as the source intensity. The intensity results are reflected also in the average distance between the center of the focal volume and the particle during the tracking runs is shown in Fig. 10c.

5.8 Discussion

While a rate of 4.4 million counts/s is extremely high, the results serve to illustrate the tradeoff between tracking speed and fluorescence intensity. In essence, the controller must be fast enough to react to the particle motion and must receive enough photons within each cycle to infer information about that motion. For faster moving particles, it is important to have fast controller update rates so as to react to the particle motion and keep it inside the detection volume. As the controller rate is increased, and correspondingly as the measurement integration time is decreased, the number of counts per measurement decreases. If the measurement time becomes too small, then there will not be enough information in the signal to drive the tracking algorithm.

Such a tradeoff is common across any tracking technique. The results found here compare favorably in terms of tracking speed to the results in the literature. It should be noted, however, that there are several effects not modeled in these simulations that would likely have a detrimental effect on the tracking performance. These include differences between the ideal PSF modeled here and the PSF of real objective lenses [30], nonlinear effects in the piezo actuators [22], and additional noise sources in the electronics. Because the control law (10c) depends explicitly on differences in the measured intensity, fluctuations in the power of the excitation laser [31] will also be directly coupled into the tracking commands. Furthermore, in many applications, the source particle is a quantum dot. These particles blink on and off with a power law distribution of off and on times [32]; an effect not captured by the Poissonian statistics modeled here and which leads to higher noise in the measurements.

Tracking of freely diffusing particles also be limited by the range of travel of the actuators. Typically, the optical axis is the one with the shortest travel. For an actuator with a travel on the order of 10 μm, the expected first passage time is $T = 100/(2D)$ where D is the diffusion coefficient. For large values of D, this time may be much shorter than the expected tracking times of the algorithm.

6 Conclusions

In this paper, we have introduced a nonlinear algorithm for tracking single fluorescent molecules in a confocal setup. The method is entirely algorithmic and does not rely on any a priori knowledge about the optical setup, making it easy to implement. Simulation results indicate that the method can track reliably at low signal levels and, with sufficient fluorescence intensity, can track particles with very high diffusion coefficients. The effect of control parameter choice was explored in simulation, though a theoretical understanding of these parameters on the tracking efficacy is needed to optimize their selection.

The algorithm can be further improved by optimizing the choice of controller parameters to achieve the best tracking performance. Given the tradeoff between fluorescence intensity, photobleaching, and tracking ability, it is likely that an adaptive approach in which both excitation power as well as controller parameters are updated based on estimated values of parameters such as the diffusion coefficient will increase the effectiveness.

Acknowledgements This material is based upon work supported by the National Science Foundation under Grant No. CMMI-0845742.

References

1. K.I. Mortensen, L.S. Churchman, J.A. Spudich, H. Flyvbjerg, Nat. Methods **7**, 377 (2010)
2. J. Chao, S. Ram, E.S. Ward, R.J. Ober, Opt. Express **17**, 24377 (2010)
3. E.J.G. Peterman, H. Sosa, W.E. Moerner, Annu. Rev. Phys. Chem. **55**, 79 (2004)
4. E.S. Yeung, Annu. Rev. Phys. Chem. **55**, 97 (2004)
5. W.E. Moerner, Proc. Natl. Acad. Sci. USA **104**, 12596 (2007)
6. H. Yang, Curr. Opin. Chem. Biol. **14**, 3 (2010)
7. V. Levi, Q. Ruan, E. Gratton, Biophys. J. **88**, 2919 (2005)
8. K. McHale, A.J. Berglund, H. Mabuchi, Nano Lett. **7**, 3535 (2007)
9. Z. Shen, S.B. Andersson, in *Proc. IEEE Conference on Decision and Control* (2009), pp. 6052–6057
10. Z. Shen, S.B. Andersson, IEEE Trans. Control Syst. Tech. (2010). doi:10.1109/TCST.2010.2067449
11. H. Cang, C.M. Wong, C.S. Xu, A.H. Rizvi, H. Yang, Appl. Phys. Lett. **88**, 223901 (2006)
12. H. Cang, C.S. Xu, D. Montiel, H. Yang, Opt. Lett. **32**, 2729 (2007)
13. G.A. Lessard, P.M. Goodwin, J.H. Werner, Appl. Phys. Lett. **91**, 224106 (2007)
14. N.G. Walter, C.-Y. Huang, A.J. Manzo, M.A. Sobhy, Nat. Methods **5**, 475 (2008)
15. H. Cang, C.S. Xu, H. Yang, Chem. Phys. Lett. **457**, 285 (2008)
16. N.P. Wells, G.A. Lessard, J.H. Werner, Anal. Chem. **90**, 9830 (2008)
17. S.B. Andersson, in *Proc. American Control Conference* (2010), pp. 4981–4986
18. D. Baronov, J. Baillieul, in *Proc. American Control Conference* (2007), pp. 2141–2146
19. D. Baronov, J. Baillieul, in *Proc. American Control Conference* (2008), pp. 678–683
20. D. Baronov, S.B. Andersson, IEEE Trans. Nanotechnol. **9**, 367 (2010)
21. J.E. Jonkman, E.H.K. Stelzer, in *Resolution and Contrast in Confocal and Two-Photon Microscopy* (Wiley-Liss, New York, 2002), pp. 101–125
22. D. Croft, G. Shed, S. Devasia, J. Dyn. Syst. Meas. Control **123**, 35 (2001)
23. Y. Wu, Q. Zou, IEEE Trans. Control Syst. Technol. **15**, 936 (2007)
24. D.Y. Abramovitch, S. Hoen, R. Workman, Asian J. Control **11**, 188 (2009)
25. D.Y. Abramovitch, S.B. Andersson, L.Y. Pao, G. Schitter, in *Proc. American Control Conference* (2007), pp. 3488–3502
26. G. Klein, Proc. R. Soc. Lond. Ser. A, Math. Phys. Sci. **211**, 431 (1952)
27. S.B. Andersson, Opt. Express **16**, 18714 (2008)
28. S. Inoué, in *Handbook of Biological Confocal Microscopy*, 3rd edn. (Springer, Berlin, 2006), pp. 1–14
29. G.F. Franklin, J.D. Powell, A. Emami-Naeini, *Feedback Control of Dynamic Systems*, 6th edn. (Pearson Education, Upper Saddle River, 2010)
30. R. Juškaitis, in *Handbook of Biological Confocal Microscopy*, 3rd edn. (Springer, Berlin, 2006), pp. 239–250
31. E. Gratton, M.J. vandeVen, in *Handbook of Biological Confocal Microscopy*, 3rd edn. (Springer, Berlin, 2006), pp. 239–250
32. M. Kuno, D.P. Fromm, H.F. Hamann, A. Gallagher, D.J. Nesbitt, J. Chem. Phys. **7**, 3117 (2000)